Driving-Cycle Oriented Design Optimization of a Permanent Magnet Hub Motor Drive System for a Four-Wheel-Drive Electric Vehicle

Xiaodong Sun, *Senior Member, IEEE*, Zhou Shi, Yingfeng Cai, *Member, IEEE*,
Gang Lei, *Member, IEEE*, Youguang Guo, *Senior Member, IEEE*, and Jianguo Zhu, *Senior Member, IEEE*

***Abstract*- The electrical drive system is crucial to the drive performance and safety of electric vehicles (EVs). In contrast to the traditional two-wheel driven EVs, the hub motor four-wheel-drive system can steer the vehicle by controlling the torque and speed of each wheel independently, yielding a very simple distributed drivetrain with high efficiency and reliability. This paper presents a system-level design optimization method for a permanent magnet hub motor drive system for a campus patrol EV based on a practical driving cycle. An outer rotor permanent-magnet synchronous hub motor (PMSHM) and an improved model predicate current control are proposed for the drive system. Due to the lack of reducers, the direct-drive PMSHM needs to face more complex working conditions and design constraints. In the implementation, the motor design requirements are obtained through the collection of practical EV driving cycles in the campus. Based on these requirements, two models are proposed as the preliminary designs for the PMSHM. To improve their performance, an efficient multi-objective optimization method is employed to the motor considering different operational conditions. The finite-element model and thermal network model are employed to verify the performance of the optimized PMSHM. An optimal design scheme is selected by comparing the comprehensive performance of the two optimized motors. In addition, a duty-cycle model predictive current control is adopted to drive the motor. Finally, a prototype is developed and tested, and the experimental results are presented.**

Keywords: Electric vehicles (EVs), permanent-magnet synchronous hub motor (PMSHM), Multi-objective optimization, model predicate current control.

I. Introduction

As the environmental issues are on the rise in the automotive industry, the market share of the new energy vehicles, which include hybrid electric vehicles (HEVs) and pure electric vehicles (EVs) that are powered by electric motors as the traction component is getting larger and larger. Modern EVs require high-performance drive motors with high torque density and efficiency. Many kinds of motors have been studied and developed for this purpose, such as permanent magnet synchronous motors (PMSMs), switched reluctance motors and induction motors [1-5]. The majority of these EVs, however, are two-wheel drive on either the front or rear axle by a single motor. The dynamic performance of such a two-wheel drivetrain is sub-optimal due to the limited traction and regenerative braking capability, especially when it is riding on roads with snow and/or ice, or off-road on soft grounds or rocks. The four-wheel-drive drivetrain using four hub/in-wheel motors can overcome this drawback. Since the torque and speed of each wheel can be controlled independently. Different from centralized drive motors, the requirement of light weight is stricter for hub motors since the mass of the hub motor will affect the unspring mass, which has a significant impact on the ride comfort of the EVs. Due to the characteristics of low speed stability, high torque density, and low torque ripple, the PMSM is a good candidate for the EV hub motor.

To have a good design of EV hub motor, driving conditions and optimization are always required and have been investigated in many researches. Regarding the driving conditions, many researches employed the new European driving cycles (NEDC) and in [6], NEDC was divided into six different driving conditions for further study. In [7], the rotation speed and phase current of a high-speed PMSM on one urban and highway cycle was investigated from NEDC. Some other drive cycles such as Federal Test Procedure (FTP), Urban Dynamometer Driving Schedule (UDDS) and JC08 are also studied in many researches on the motor design. Besides, there are also some researches on the design of permanent magnet machines based on the driving cycle [8-12]. These studies are mainly to determine the initial design parameters by studying the body parameters and cycle conditions, mainly in determining the demand torque and speed range. However, more information can be expressed in the cycle condition. This paper aims to optimize the efficiency of the motor under the whole cycle condition by analyzing the working points of the cycle condition, combining the efficiency of each working point with the use frequency.

Motor optimization is a complex nonlinear optimization problem. The main optimization algorithms can be divided into two categories: gradient-based algorithms and optimization algorithms based on non-analytical machine

X. Sun, Z. Shi, and Y. Cai are with the Automotive Engineering Research Institute, Jiangsu University, Zhenjiang 212013, China (email: xdsun@ujs.edu.cn, shizhoujiangda@163.com, caicaixiao0304@126.com). *(Corresponding author: Yingfeng Cai)*

G. Lei and Y. Guo are with the School of Electrical and Data Engineering, University of Technology Sydney, NSW 2007, Australia (e-mail: Gang.Lei@uts.edu.au, Youguang.Guo-1@uts.edu.au).

J. Zhu is with the School of Electrical and Information Engineering, University of Sydney, NSW, 2006, Australia (e-mail: jianguo.zhu@sydney.edu.au).

models. Gradient-based algorithms, such as conjugate gradient algorithm, sequential quadratic programming algorithm and augmented Lagrange multiplier method. Generally, the first or second order derivative or Hessians matrix is required in the implementation. To use these algorithms efficiently, there are several constraints, such as: the objective functions should be continuous and derivable; the objective functions and constraints can be expressed analytically; and the constrained optimization models have to be converted to unconstrained forms for some initial gradient-based algorithms, e.g. the conjugate gradient algorithm. Analytical models or methods for electromagnetic, thermal, and other disciplinary analyses should be constructed before the optimization. However, many analysis models for electrical machines are based on FEM, and there is no analytical expression for the optimization model. Therefore, various intelligent optimization algorithms using non-analytical machine models have been employed, such as those based on the Genetic Algorithm (GA) and Partical Swarm Optimization (PSO) algorithms. Optimization methods based on GA and PSO algorithms also has shortcoming of the huge computation cost of FEM when the dimension of optimization problem is high. Therefore, Kriging model is adopted in the non-dominated sorting genetic algorithm II (NSGA II) progress to simplify the complicated finite element calculation process.

In the aspect of control methods for PMSHM, there are various kinds of applied in PMSHM drives such as field-oriented control (FOC) and direct torque control (DTC) [13-18]. FOC and DTC also have their shortcomings. In the one hand, FOC needs to tune the parameters which will affect the real drive performance. In the other hand, DTC generates high torque and flux ripples and high switching frequency causes the hardware loss. Compared the conventional control, model predictive control (MPC) selects the optimal voltage vector by minimizing the error between the reference value and predictive value. And it carries out rolling optimization to achieve the better performance. Hence, MPC is more precise and high efficiency than DTC and FOC. Meanwhile, model predictive current control (MPCC) has been presented for the selection of stator current and widely regarded as a powerful control strategy for PMSM drives. Therefore, duty-cycle model predictive current control (DCMPCC) will be studied as the control strategy for the proposed motor.

This paper aims to study the design principles and multi-objective optimization of an outer rotor PMSHM based on the actual operational conditions. In addition, a non-dominated sorting genetic algorithm II (NSGA-II) and Kriging models will be used to optimize the parameters of this PMSHM, which will decrease computation time significantly. Besides, duty-cycle model predictive current control will be used to achieve higher steady-state performance and quicker response to a greater extent. In addition, the improved control strategy also can reduce torque and current ripples.

The main contributions of this paper can be summarized in the following.

(1) A system-level design optimization method is presented for a permanent magnet hub motor drive system for a campus patrol EV, which can be regarded as an example of driving-cycle oriented design optimization method for EVs.

(2) In order to achieve a higher steady-state performance and have a quicker response, an improved DCMPCC is presented in this paper which has remarkable effect on reducing phase current ripples and improving steady state performance. The main improvements are by introducing the zero vector, the output of the controller can be the duty ratio of the optimal non-zero vector, so the output voltage of the controller can be closer to the reference voltage in the amplitude, the current ripple can thus be reduced. Also, two zero vectors can be used to compose output voltage, so the switching times can be reduced by selecting the appropriate zero vectors.

The remainder of the paper is organized as follows. Section II shows the data of an actual driving cycle and investigates the design principles for the PMSHM. Section III presents the flowchart and details for the multi-objective optimizing of this PMSHM. Section IV shows the Pareto optimal solutions and discusses the choosing method of a final optimal design based on them. Section V shows the experimental results on a prototype and the comparisons between simulated and measured results, followed by the conclusion.

II. Multi-Objective Optimization Strategy

In this paper, to ensure the designed PMSHM can meet all the requirements of the test EV, the systematic multi-objective design optimization of an PMSHM is proposed. As there is no transmission system on a hub motor drive EV, the operation condition of the PMSHM is much more complex. The requirements of the torque range and speed range increased substantially. In the proposed systematic multi-objective design optimization method both the motor structure and the motor control should are required to be considered. As shown in Fig. 1. the progress of the systematic multi-objective design optimization of the PMSHM can be arranged as follow.

Firstly, according to the application scenarios of the test EV, the speed range, maximum slope, and the high frequency working condition need to be analyzed. Then, the application requirements including speed range, maximum torque, efficiency, and constraints for the PMSHM can be decided based on the driving cycle analysis and EV body parameters.

Secondly, on the motor design progress the initial specifications of the PMSHM can be derived according to the design theory and experience. Besides, the multi-objective optimization of the PMSHM will be carried out for a better comprehensive performance.

Thirdly, based on the concept of conventional MPCC, a duty-cycle MPCC has been adopted. The original cost function will be changed for better control performance. Then, the optimal voltage vector and duty cycle can be selected to satisfy the requirement.

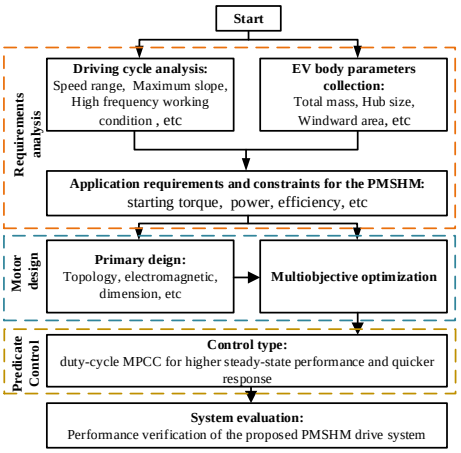

Fig. 1. Multi-objective Optimization and Predicate Control.

III. PRELIMINARY MOTOR DESIGN

3.1. Road condition

The PMSHM studied in this paper is designed for a campus patrol EV, which has a relatively fixed cycle condition. In this research, the driving cycle of campus patrol cars is sampled and shown in Fig. 2. The maximum slope is 12%. The required operation points including torque and rotation speed of the PMSHM are calculated through (1) and (2).

$$n=\frac{1000\cdot u_{\mathrm{a}}}{60\cdot 2\pi R_{\mathrm{W}}} \tag{1}$$

$$T_r=\frac{1}{4}\frac{R_{\mathrm{w}}}{\eta}\left(Gf\cos\alpha_1+\frac{C_{\mathrm{D}}A}{21.5}u_{\mathrm{a}}{}^2+G\sin\alpha_1+\delta m\frac{\mathrm{d}u_{\mathrm{a}}}{\mathrm{d}t}\right) \tag{2}$$

where R_{w} is the tire radius, u_{a} is the speed of the vehicle, α_1 is the road slope which can be calculated by the horizontal height of the road and the speed of the EV, G (G=g**m*v where g=9.803 m/s2) and f are the gravity friction resistance coefficient of the EV respectively, C_{D} and A are the drag coefficient and windward area, respectively, and δ is the coefficient of the revolving mass changes to linear mass, δm is (m u_{a} +*Jw*/*rw*^2). The unit of u_{a} is km/h and the rest units are all standard international units. And the parameter values of the test EV are given in Table I.

Table I. The Parameter Values of The Test EV

Parameters	Symbol	Value
Total mass of the EV	m	900 kg
Front cross sectional area	A	2.1 m^2
Air drag coefficient	C_D	0.34
Rolling friction coefficient	f	0.015
Radius of wheel	R	0.275m
Coefficient of the revolving mass	δ	1.05

Fig. 3 shows the main operation points of the EV in the driving cycle. As shown, these working points can be classified into the following categories: starting condition, low speed climbing, medium speed cruise, and high-speed cruise. The requirement of maximum torque of the motor needs to be larger than 100 Nm, the maximum speed of the motor needs to be more than 600 rpm, the low-speed operation is around 280 rpm, and the high-speed operation is around 530 rpm.

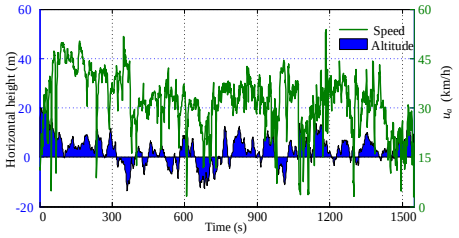

Fig. 2. Speed and horizontal height profiles of an EV route.

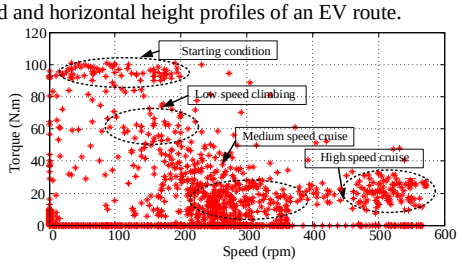

Fig. 3. Working points of the EV during the driving cycle.

3.2. Sizing and Winding Structure of the Outer Rotor PMSHM

For designing an outer rotor PMSHM, the size of the motor is limited by the space of hub. It requires the motor to be designed with high torque density in a fixed space to meet the speed requirements.

There are several principles to follow when designing an outer rotor hub motor:

(a) Maximizing diameter-length ratio.

Different from the cylindrical shape of conventional motors, the outer rotor hub motors have a larger diameter while sum length of the height of rotor yoke, height of stator yoke, height of stator tooth, and PM thickness is significantly smaller than the hub radius. Therefore, the geometry of the outer rotor hub motors can be equivalent to a ring [19]. The volume of a toroidal motor meets

$$Mass\propto Volume_{\mathrm{toriod}}\propto(D_{so}l_{Fe}) \tag{3}$$

where D_{so} is the stator outer diameter, l_{Fe} is the iron core length. For a given magnetic field strength, the torque can be achieved by positioning the air-gap against the assumed largely cylindrical outer surface of the motor. Hence, the peak torque (T_{peak}) of the outer rotor PMSHM meets

$$T_{\mathrm{peak}}\propto(D_{\mathrm{so}}{}^2l_{Fe}) \tag{4}$$

Substituting (3) into (4) gives

$$\frac{T_{\mathrm{peak}}}{Mass}\approx D_{\mathrm{so}} \tag{5}$$

It can be concluded that a larger diameter and minimum axial length, toroidal form motor can provide the maximum torque-mass ratio. Without considering the influence of leakage of the PM field and end winding larger diameter and minimum axial length motor structure is much suitable for the design.

(b) Choosing suitable slot/pole numbers.

Since there is no transmission system in the hub, the requirement of output torque of the PMSHM is relatively high. Hence, it is necessary to use a high number of pole pairs to ensure the torque density. However, high number of pole pairs will cause high electrical frequency. The high electrical frequency has several drawbacks: high iron losses in the stator, high additional ac losses in the stator winding, and that most of commercial frequency converters become improper. Therefore, choosing suitable slot/pole numbers for the motor is of great importance.

(c) Adopting suitable winding structure.

Two-layer concentrated fractional slot winding structure is chosen for the motors, since the end winding of this winding structure is short, which can reduce the copper loss and save the space. Furthermore, a large pole number is usually adopted in hub motor to improve the torque density. Fractional slot winding can reduce the length of end winding effectively, hence factional winding is often adopted.

Combining the speed and height profiles of the EV route with (1) and (2), the operational rotation speed range of the PMSHM is 0-600 rpm. The design speed range is 0-800rpm considering that the speed can be faster under better road conditions. The speed of medium speed cruise is around 300 rpm, the speed of high-speed cruise is around 520 rpm, and the peak torque should reach 100 Nm. In addition, the DC voltage of the EV is 72 V.

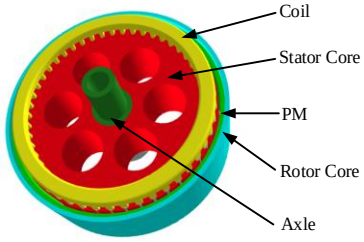

Fig. 4. 3D geometry of the PMSHM.

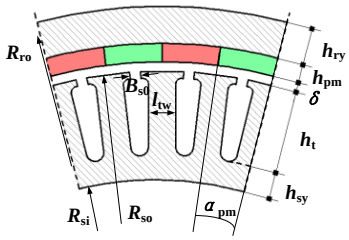

Fig. 5. Key dimensions of an outer rotor PMSHM.

The 3D geometry of the PMSHM studied in this paper is shown in Fig. 4, including the coils, stator core, PM, rotor core, and axle. The endcap and bearings are not shown in the figure. It has been concluded that toroidal motor can provide the maximum torque-mass ratio with a larger diameter and minimum axial length. However, the diameter of the PMSHM is also limited by the hub inner diameter. In addition, the motor and hub are designed to be bolted, instead of an integral EV hub, so a certain stator heat dissipation space needs to be set aside. Therefore, the hull size of hub motor is initially determined to be 235 mm, the rotor outer diameter is determined to be 220 mm, and the air gap diameter is determined as 199 mm. According to the peak torque requirement and air gap diameter, the iron length of the motor is initially determined to be 55 mm, which meets the demand of hub space.

The two initial slot and pole numbers adopted in this design are both multi pole fractional slot rotors. Fractional slot winding can reduce the end winding and torque ripple effectively. And high pole number is good for improving magnetic density. Besides, motor with close pole and slot motor is a hot spot in recent years due to its characteristics of high efficiency, high power density, short end winding, low torque ripple and good demagnetization ability. Regarding the slot/pole numbers of the PMSHM, two initial schemes are determined, which are 46/48 and 50/51 poles/slots. Besides, the winding structure of the two models are different; the double layer winding is used in the 50/51 model and the single layer winding is adopted in the 46/48 model. In the next optimization design process, both schemes will be taken as optimization objectives and the results of them will be compared to select the appropriate slot/pole numbers for a final scheme for the prototype.

Table II. Parameters of two initial models

Parameters	Sym./Unit	Model I	Model II
PM thickness	h_{PM}/mm	4	4
Number of poles	P	46	50
Number of stator slots	Z	48	51
Rotor yoke height	h_{ry}/mm	8	8
Height of stator tooth	h_t/mm	15.8	16.0
Stator tooth width	l_{tw}/mm	6	5.6
Height of rotor yoke	h_{ry}/mm	6.3	6.2
Height of stator yoke	h_{sy}/mm	5.4	5.2
Fill factor	N/A	< 0.62	
Current density	A/mm^2	< 13	
Winding turns	N/A	20	

The key design parameters of the outer rotor PMSHM are shown in Fig. 5, where R_{ro} and R_{si} are the rotor outer radius and stator inner radius, respectively, h_{ry} and h_{sy} are the height of rotor yoke and height of stator yoke, respectively, h_t is the height of stator tooth, l_{tw} is the stator tooth width, δ is the air gap length, and h_{pm} is the PM thickness. The initial design parameters of the two models of PMSHMs with different pole and slot numbers are listed in Table II. Fig. 6 shows the FEMs for the two motors.

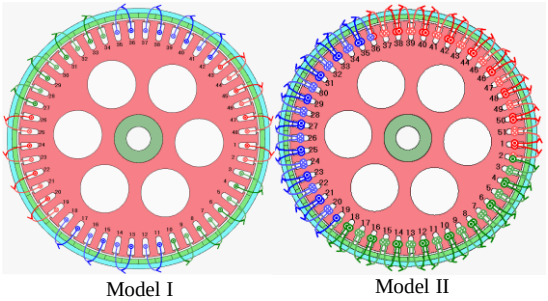

Model I Model II

Fig. 6. Initial FEM with different winding distribution of two models.

Table III. Design parameters and values of two models for optimization

Model I (46 poles/48 slots)			
Parameters	Sym./Unit	Initial	Range

Stator tooth width	l_{tw}/mm	5.80	(5.0-7.0)
Height of stator tooth	h_t/mm	15.8	(15-19)
Slot opening	B_{s0}/mm	1.80	(1.6-2.4)
PM arc coefficient	$51*\alpha_{PM}/2\pi$	0.85	(0.8-1.0)
Model II (50 poles/51 slots)			
Parameters	Sym./Unit	Initial	Range
Stator tooth width	l_{tw}/mm	5.60	(4.8-6.8)
Height of stator tooth	h_t/mm	16.0	(15-19)
Slot opening	B_{s0}/mm	1.80	(1.6-2.4)
PM arc coefficient	$51*\alpha_{PM}/2\pi$	0.85	(0.8-1.0)

IV. MULTI-OBJECTIVE OPTIMIZATION IN MOTOR LEVEL

4.1. Optimization Model, Objectives, and Constraints

As shown in Fig. 5, the motor has many design parameters. In this work, six parameters will be considered in the process of design optimization. They are the stator tooth width h_t, height of rotor yoke h_{ry}, height of stator yoke h_{sy}, PM pole arc angle coefficient $51*\alpha_{PM}/2\pi$, PM thickness h_{PM}, and the stator tooth width l_{tw}. To reduce the optimization parameters and improve the optimization efficiency, some constraints are applied to these parameters. First, since h_{sy}, l_{tw} and h_{ry} are mainly affected by the magnetic flux density B, it would be reasonable to optimize the l_{tw} while keeping $h_{sy}/l_{tw}=C_1$, $h_{ry}/l_{tw}=C_2$. Second, it is necessary to keep the same mass of PMs in the design process, $\alpha_{PM}\cdot h_{PM}=C_3$ is applied. By keep *C1*, *C2* and *C3* are fixed can ensure the flux density in stator teeth, stator yoke, and rotor yoke the same. With this setting, the number of parameters to be optimized can be reduced. R_{ro}, R_{so}, R_{si} keep constant in the optimization progress. They are determined by the initial design. Through these two steps, there are four parameters to be optimized. As the amount of PM and outer diameter are determined, the other parameters can be expressed by these four parameters. After the preliminary calculation, the ranges of these four parameters are listed in Table III.

In the progress of primary design of the PMSHM the driving-cycle has been taken into consideration. In the process of determining optimization objectives and constraints, it is also necessary to take driving-cycle into consideration. In order to ensure that the vehicle has good starting performance, a larger starting torque is needed. Torque ripple is also another important optimization objective as it has a great influence on ride comfort especially in the starting condition. Efficiency under rated operating condition is the main consideration in traditional motor optimization. However, as there is no transmission system for a hub motor drive system, the operating range of motor is large. If there is a transmission system, the drive motor can be kept in a relatively efficient speed area by adjusting the transmission ratio. However, due to the lack of the working point of the drive system motor in the hub drive EVs, it is directly related to the cycle condition, so the motor needs to be kept in a more efficient condition area. Therefore, it is necessary to optimize the comprehensive efficiency (f_3) which take efficiency under different working condition into consideration. The multi-objective optimization model can be developed as follows.

$$\min: \begin{cases} f_1(x) = -T_{\max} \\ f_2(x) = T_{ripple}\% \\ f_3(x) = 1/\sum_{i=1}^{4} \hat{f}_i \eta_i \end{cases}$$
$$\text{s.t.} \begin{cases} g_1(x) = T_{\max\_initial} - T_{\max} \le 0 \\ g_2(x) = T_{\text{ripple}} - T_{\text{ripple\_initial}} \le 0 \\ g_3(x) = \Delta T_{\text{core}} \le T_{\text{core max}} - T_{\text{initial}} \\ g_4(x) = \Delta T_{\text{winding}} \le T_{\text{winding max}} - T_{\text{initial}} \end{cases} \quad (6)$$

where $T_{\max}$ and T_{ripple} are the maximum torque and torque ripple of the PMSHM, respectively. $T_{\max}$ is achieved under a current density of 13 A/mm^2. η_i and $\hat{f}_i$ are the efficiency and frequency of the ith operational condition, respectively. In this optimization four operational conditions are calculated as listed in Table IV.

To unify the objectives into the minimum optimum negative maximum torque and reciprocal of comprehensive efficiency are adopted. The losses in the motor is calculated by ANSYS 2D model. The calculation of the loss of end winding is realized by inputting the end length in the two-dimensional finite element. Temperature does influence loss, but it is not considered in this study.

Table IV. Design Parameters of Initial and Optimized Models

	Speed (rpm)	Torque (N.m)	Frequency (%)
Point 1	110	95	11
Point 2	170	60	10
Point 3	300	18	59
Point 4	530	24	20

In the optimization process of PM motors, the main optimization objectives are the maximum torque and minimal torque ripple. Regarding the efficiency, most studies use the efficiency of the rated working condition. However, the working conditions of EVs are relatively complex, and the efficiency under rated working conditions cannot express the efficiency under the whole driving cycle effectively. It seems reasonable to calculate the efficiency of the whole driving cycle. However, in the optimization process, the efficiency of the whole cycle needs a lot of calculation which will result in huge computation cost for the multi-objective optimization. Besides, the efficiency is not the most important objective in some working conditions such as the start-up and climbing. In this study, the efficiency of a typical point under low speed condition and the efficiency of a typical point under high-speed condition are weighted as the overall efficiency as show in $f_3(x)$. The Pareto boundary is used to select the optimal results. The related temperature network establishment methods can be referred to [20, 21].

The combined efficiency is close to the real efficiency during the whole drive cycle. ΔT_{core} is the temperature rise in the stator core as the stator core loss will cause high temperature rise in the stator. The ΔT_{core} is calculated under the working condition of 500 rpm 30 Nm and takes 250 seconds which considers the condition of the highest speed and full load operation. $\Delta T_{\text{winding}}$ is the temperature rise in the

winding. The $\Delta T_{winding}$ is calculated under the working condition 50 rpm 90 Nm and takes 100 seconds which considers the condition of the speed up working condition. Considering the working temperature of coils and stator core will affect the loss of the motor, the temperature constraints of the windings ($T_{coremax}$) and stator core ($T_{windingmax}$) are 100 °C and 90°C. $T_{initial}$ is the initial temperature of the motor which is set to be 40 °C in this study.

The constraints adopted in this study include the maximum torque, and torque ripple and temperature rise. Maximizing torque and minimizing torque ripple can be easily calculated through FEM. In addition, temperature rise is also the main constraint in the design process of this hub motor. Temperature limit usually occurs in the following two conditions. One is the start-up condition, in which the loss is mainly caused by high current density. The other is the high-speed cruise, in which the power loss is mainly caused by both iron loss and copper loss. The winding temperature rise, and stator temperature rise reach their maximum values under these two working conditions, so when setting constraints, the winding temperature rise and stator tooth temperature rise under these two conditions are calculated. When calculating the temperature rise, it is necessary to import a large number of loss parameters from the electromagnetic FEM and establish temperature field models to calculate temperature rise, which will make the operation of optimization design complicated. Thus, a simplified temperature network model is used in this study as show in Fig. 7. As shown, the equivalent thermal resistances of the axle, stator yoke, stator teeth, phase winding, end winding, air, PMs, rotor, housing, and endcap are represented in square. The heat sources in this model include the stator core loss (*P*stator), rotor core loss (*P*rotor), phase winding loss (*P*cu1, *P*cu2, *Pcu*3), end winding loss (*Pcu*End1, *Pcu*End1), and PM eddy current loss (*P*PM). All the losses are calculated by the FEM. The ΔT_{core} and $\Delta T_{winding}$ can be calculated through the temperature network.

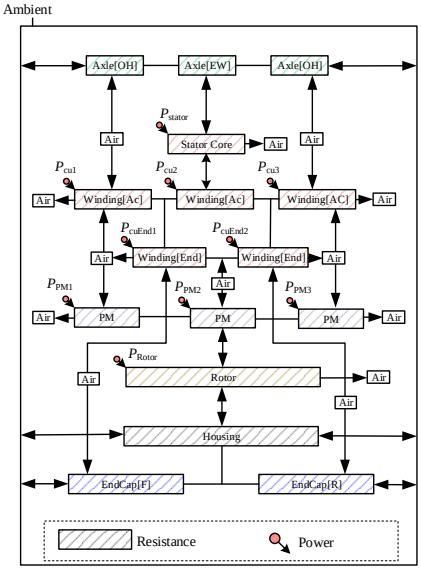

Fig. 7. Thermal network model of the outer rotor PMSHM.

4.2. Multi-objective Optimization Method

A. Kriging model

Through the FEM and temperature network model all the optimization objectives and constraints can be calculated as introduced. However, the computational cost of FEM is very high, especially for motor with complex structure. As an alternative, some approximate models are used in practical engineering design to reduce the computational burden of optimization process.

Kinging is chosen to construct the approximate multi-objective optimization models to reduce the FEM computation cost of PMSHM in this work. Kriging is a semi-parameter model whose response value incorporates a mean trend term and a variance term as

$$y(x) = y_0(x) + z(x) \tag{7}$$

where $y_0(x)$ can be a response surface model (RSM), such as linear polynomial and quadratic polynomial, $z(x)$ is the error function which is generally defined as a vector variable with mean zero, variance σ^2 and covariance matrix $C_w=[c_{ij}]$ as

$$c_{ij} = \sigma^2 \mathrm{R}\left[\Re\left(x_i, x_j\right)\right] \quad i, j = 1, 2, \cdots n \tag{8}$$

where x_i and x_j are sample points, R is the correlation matrix, $\Re$ is a correlation function. Kriging model is claimed to be superior in the modeling of local nonlinearities and has been widely used in design of electromagnetic devices [22].

B. Multi-objective optimization model

For the multi-objective optimization of model (6), it can be done by using the conventional multi-objective optimization framework. For example, optimizing all parameters by using the multi-objective genetic algorithm (MOGA). However, the required FEM will be 30,000 (100*300) assuming that 100 is the population size in each iteration and 300 is an average iteration of the algorithm to reach convergence. This is a huge computation cost, especially in the case of PMSHM with a pole number requiring small meshes. Therefore, to decrease the computation cost of finite element analysis (FEA), a multi-objective sequential optimization method (MSOM) will be employed in this work [23]. Fig. 8 shows a flowchart of this MSOM, and it mainly includes five steps as follows. There are four parameters to need to be optimized they are stator tooth width, height of stator tooth, slot opening and PM arc coefficient.

1) Initialize the input data and acquire the corresponding output data through the FEA and build Kringing model through these data.

2) Generate an initial sample set S(0) and obtain initial Pareto optimal solution P(0) using NSGA II. NSGA II is a classic multi-objective optimization algorithm, which can be used to optimize model or its approximate model to provide Pareto optimal solution. A controlled elitist multi-objective genetic algorithm (MOGA, a variant of NSGA II) in Matlab is adopted in this work. Except the population size, the other algorithm parameters are the default values, e.g., Pareto fraction is 0.35. 100 is defined for population size as there are three optimization objectives in this work.

3) Update the samples based on the obtained Pareto optimal solutions. To improve the modeling efficiency, a

modified central composite design (CCD) sampling method is presented to update the sample sets. The CCD is a classic sampling method for the construction of RSM. It divides the samples into two subsets, one for the property estimation of the linear term, and the other for the curved surface. It is claimed to be superior in the modeling of RSM. With these new samples, all the Kriging models can be updated.

4) Optimize the obtained Kriging model using NSGA II and get updated Pareto optimal solution P(k).

5) Determine if P(k) is the final Pareto solution. Compute the root-mean-square error (RMSE) of the obtained Pareto points for each Kriging model. If all RMSEs are no more than ε (1% by default), output the solution, otherwise go to step 3.

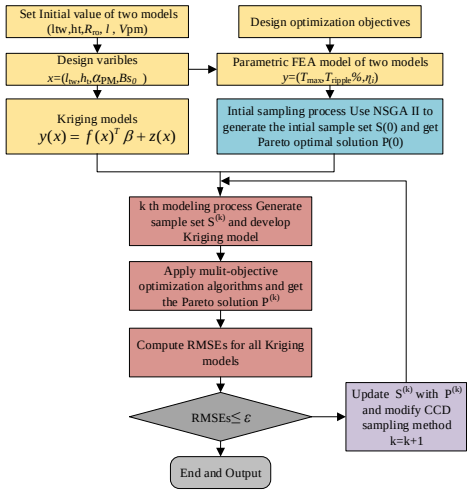

Fig. 8. Flowchart of the whole optimization progress.

4.3. Optimization Results

A. Results of MSOM

The needed FEM sample points of MSOM are 636, which is only 2.12% compared with that required by the direct multi-objective optimization of FEM with MOGA, in which about 30,000 FEM samples are needed. Fig. 9 (a) illustrates the Pareto optimal solutions obtained from the MSOM for the three objectives of the investigated PMSHM based on model (6). To clearly show the Pareto front, the projections of the solutions in the 2D planes are shown in Figs. 9 (b)-(d).

To show the optimization efficiency of the proposed MSOM and compare the motor performance between the optimized and initial designs, three points (design schemes) are selected and marked in Fig. 9 as well. The corresponding design parameters and performance parameters of the initial and final selected optimization result points are shown in Table V.

As shown, the performance optimized design points are obviously better than those of the initial design points. All the points in the Pareto solutions are superior to the initial design points in any optimization objective. The maximum torque can reach 117 Nm, the torque ripple could reach 3.65%, and the comprehensive efficiency could reach 92.15%. However, these three optimum values are not achieved under the same point. These three points can be considered as alternatives to the final design data for Model I.

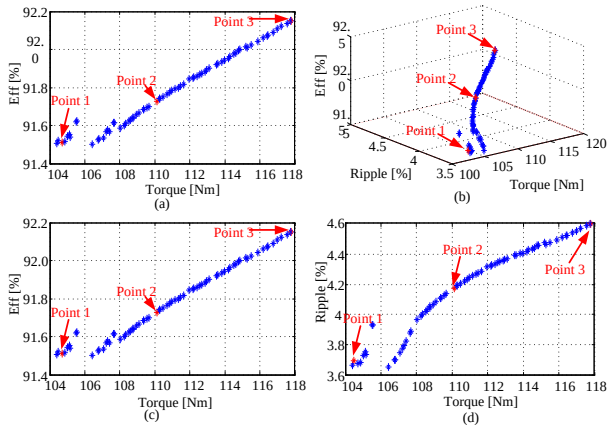

Fig. 9. (a) The Pareto optimal solution obtained from the MSOM, (b) a projection of Pareto optimal solution on torque and comprehensive efficiency, (c) a projection of Pareto optimal solution on torque ripple and comprehensive efficiency, and (d) a projection of Pareto optimal solution on torque and torque ripple.

B. Validation of the optimization

In order to verify the accuracy of the Kriging model, the FEM is used to obtain the parameters of the three alternative points. The torque curves of all four points are shown in Fig. 10 (a), which is in agreement with maximum torque and torque ripple data in Table III. Since the comprehensive efficiency cannot be shown by the finite element results, the values of iron loss and PM eddy current loss under the typical working points with the highest frequency are compared in Fig. 10 (b). The loss results are basically consistent with the comprehensive efficiency data in Table V. The above results show that the accuracy of Kriging model prediction is reliable.

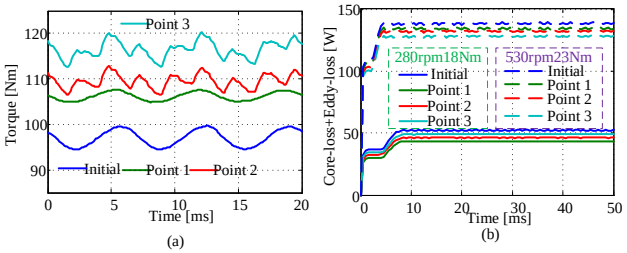

Fig. 10. Comparison of four points in FEM. (a) Maximum torque curves of initial and multi-objective optimal designs, and (b) Sum of iron loss and PM eddy current loss under two typical working points of initial and multi-objective optimal designs.

In order to verify the temperature constraint, the transient simulation of temperature field is carried out. The whole temperature field simulation process can be divided into three parts as shown in Fig. 11. The first part is the maximum torque acceleration process, which takes 100 seconds. The process is longer than the actual acceleration time, which considers that the vehicle may face some continuous climbing condition and will also work in the maximum torque state. The second part is the rated power acceleration, which takes 100 seconds. The third part is the high-speed cruising, which takes 175 seconds.

As shown, the maximum temperature of the coils can reach 92ºC under continuous maximum torque condition. This temperature is still within the safe range, so the model meets the design requirements. When the motor runs in high speed cruise condition, the temperature can reach steady state, and the temperature of the stator can reach 75ºC.

C. Choice of the final design

For Model I, point 1 is chosen as the final design parameter by comparing the results. Although the maximum torque and comprehensive efficiency of this point are slightly lower than those of the other two points, the torque ripple is smaller than those of the other two points significantly. The optimization process of Model II is the same Model I. In order to save space, the optimization process of the Model II has not been fully described. The final selected optimization result point of Model II is shown in Table V. As shown, the optimal result of Model II has the highest efficiency. However, the torque ripple of Model II is absolutely larger than the torque ripple of the Model I. Finally, Model I is selected as the final design scheme under comprehensive consideration.

Table V. Design Parameters of Initial and Optimized Models

Parameters	Sym./ Unit	Model I (46 poles/48 slots)			
		Initial	Point1	Point2	Point3
Stator tooth width	l_{tw}/mm	5.8	6.9	6.8	6.4
Height of stator tooth	h_t/mm	15.8	17.6	17.8	18.0
Slot opening	B_{s0}/mm	1.80	2.40	2.35	2.38
PM arc coefficient	α_{PM}/deg	0.85	0.89	0.98	0.98
Max. torque	T/Nm	98.4	106.0	110.0	117.0
Torque ripple	%	5.70	3.65	4.18	4.60
Efficiency	%	91.6	91.5	91.7	92.15
Parameters	Sym./ Unit	Model II (50 poles/51 slots)			
		Initial		Optimized	
Stator tooth width	l_{tw}/mm	5.6		6.7	
Height of stator tooth	h_t/mm	15.8		17.8	
Slot opening	B_{s0}/mm	1.80		2.30	
PM arc coefficient	α_{PM}/deg	0.85		0.96	
Max. torque	T/Nm	102.3		113.0	
Torque ripple	%	6.85		5.64	
Efficiency	%	91.6		92.17	

D. Choice of the final design

For Model I, point 1 is chosen as the final design parameter by comparing the results. Although the maximum torque and comprehensive efficiency of this point are slightly lower than those of the other two points, the torque ripple is smaller than those of the other two points significantly. The optimization process of Model II is the same Model I. In order to save space, the optimization process of the Model II has not been fully described. The final selected optimization result point of Model II is shown in Table V. As shown, the optimal result of Model II has the highest efficiency. However, the torque ripple of Model II is absolutely larger than the torque ripple of the Model I. Finally, Model I is selected as the final design scheme under comprehensive consideration.

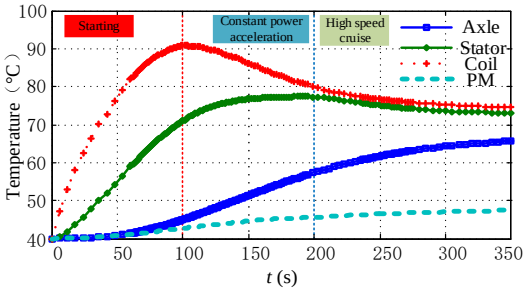

Fig. 11. Simulation results of thermal network model of the outer rotor PMSHM.

V. Duty-cycle model predicate current control

The PMSHM should have a large starting torque and a wide range of speed regulation performance to meet the required power and torque of starting, acceleration, driving, deceleration and braking. Other than the systematic multi-objective optimization, an advanced control strategy is also necessary to improve the drive performance of PMSHM. Therefore, the DCMPCC has been adopted to be applied to control the PMSHM with better effect. Compared with conventional MPCC, in which only one voltage vector will be applied in the whole control period, DCMPCC selects the best voltage and its duration, thus DCMPCC can track reference voltage more precisely. The control scheme of the DCMPCC is shown in Fig.12. More detailed comparison can be found in [24, 25]. In this section, DCMPCC will be compared with conventional MPCC in different conditions.

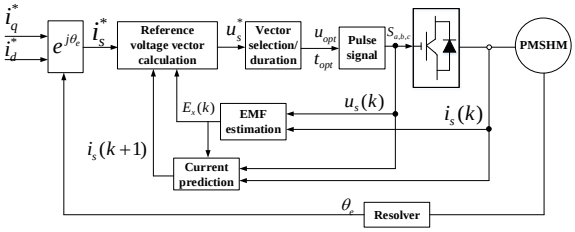

Fig. 12. DCMPCC control scheme

Compared with the conventional MPCC, DCMPCC only uses one nonzero voltage and one zero vector to reduce the computational complexity and switching frequency. In order to improve the accuracy of selecting the optimal voltage vector, the cost function is shown as follows:

$$u_s^* = R_s i_s(k+1) + L_s \frac{i_s^* - i_s(k+1)}{T_s} + E_x(k) \tag{9}$$

$$F_1 = \left| u_s^* - \frac{u_{opt} t_{opt}}{T_s} \right|^2 \tag{10}$$

where u_s, i_s and E_x= [E_α E_β]^T represent the stator voltage vector, stator current vector and back EMF in α-β frame, respectively. L_s, T_s are the stator inductance and the sampling time.

By solving the derivation of F_1 in allusion to t_{opt}, the optimal vector duration is obtained as:

$$t_{opt} = \frac{u_s^*}{|u_{opt}|^2} T_s \tag{11}$$

In order to confirm the performance of DCMPCC, some simulations have been carried out. The PMSHM starts from standstill to 300 rpm with no load. Then, the speed changes to 500 rpm at time 0.15 s, and a load torque change (from 0 Nm to 20m) is applied at time 0.35s. Fig. 13 shows the dynamic responses of two control methods. DCMPCC can reduce the torque ripple by 40%, Speed response by50%, and Current ripple by 30%.

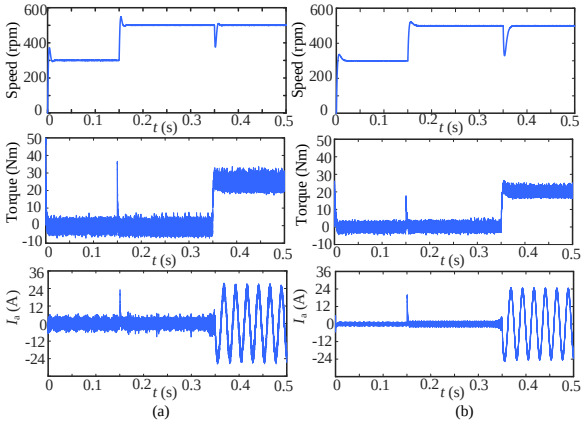

Fig. 13. Simulation starting response from standstill to 300 rpm with speed change: (a) Conventional MPCC, (b) DCMPCC

As shown, both two MPCC methods can reach the reference speed quickly. However, the conventional MPCC has a relatively large overshoot when the rotor speed reaches 300 rpm and changes to 500 rpm at 0.15 s. Meanwhile, the electromagnetic torque and phase current have significant ripples.

6. Experimental Validation

The measurement results provide essential information to verify the design of the PMSHM. A prototype of the proposed PMSHM has been manufactured, and various experiments are carried out and analyzed. Fig. 14 shows the test benches. Fig. 14 (a) is the test bench for the measurement of the no-load phase back-EMF, in which an induction motor is used to drag the prototype to measure the three-phase back-EMF of the prototyped motor at the speed of 100 rpm. The test bench for the measurement of dynamic performance includes a power source, a torque/speed sensor, a magnetic powder brake, and a motor controller based on dSPACE as shown in Fig 14 (b).

(a) (b)

Fig.14. Experimental platform configuration. (a) Test bench for the measurement of the no-load phase back-EMF, and (b) Test bench for the measurement of dynamic performance.

Fig. 15 compares the FEA-predicted and measured no-load phase back-EMF waveforms at 100 rpm. As shown, it is evident that the proposed PMSHM has sinusoidal and symmetric back-EMFs, which agrees with the FEA simulated result.

Fig. 16 shows the FEA-predicted and measured torque under different phase currents at 100 rpm. The torque measured by experiment is slightly less than that obtained by FEA, which is due to the neglect of wind resistance and mechanical loss in the simulation process.

Fig. 17 shows the temperature rise curve at 500 rpm and 40 Nm. At this working condition, the EV can keep a relatively high speed and the torque is higher than the required torque which ensures the ability of accelerating and climbing. As shown in Fig 17, at this working condition the proposed PMSHM can work at a safe temperature for 3720 seconds. The temperature can reach 138 ºC in the test which is in consistent with simulation results as the temperature sensor in stored in the winding position.

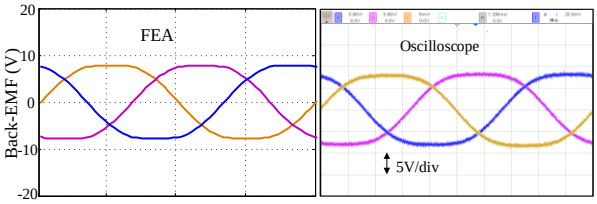

Fig. 15. No-load phase back-EMF waveforms of FEA and experiment at 100 rpm.

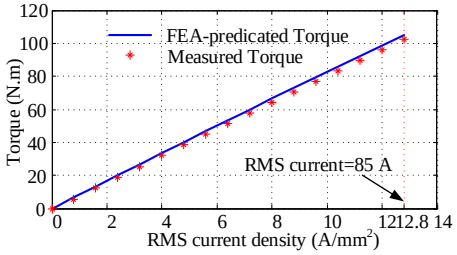

Fig.16. Measured maximum torque versus current density at 100 rpm.

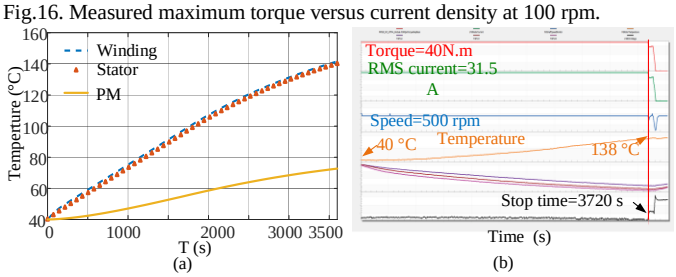

Fig.17. Temperature rise curve at 500 rpm and 40Nm (a) simulation (b) Measured.

In order to validate the simulation results of the proposed control method, the PMSHM drive experiment has been implemented via dSPACE rapid control prototyping platform. Fig. 18 shows the experimental results of PMSHM with two methods. For the fair comparison, the setting conditions are the same as the simulation in Fig. 13., starting with no-load, then a speed change at 0.15 s and a load torque change at 0.35 s.

As can be seen in Fig. 18, both two MPCC methods can reach the reference speed quickly in this no-load starting process. However, the conventional MPCC has a relatively large overshoot when the rotor speed reaches 300 rpm and

changes to 500 rpm. The dynamic performance of the MPCC is the better. For the steady-state performance, the proposed MPCC has the better performance because it has the lowest torque ripples and current harmonics

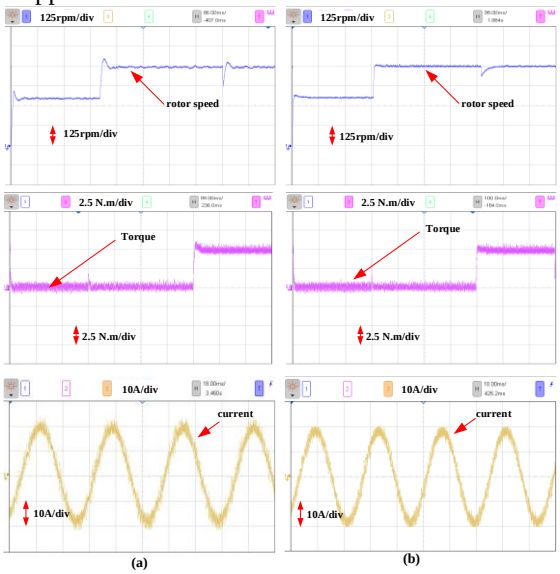

Fig. 18. Experimental starting response from standstill to 300 rpm with speed change: (a) Conventional MPCC, (b) DCMPCC

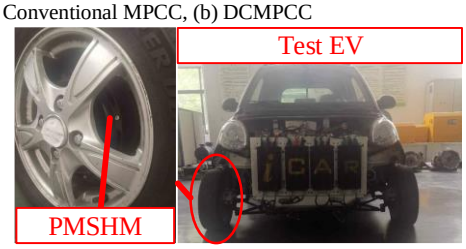

Fig.19. The test EV.

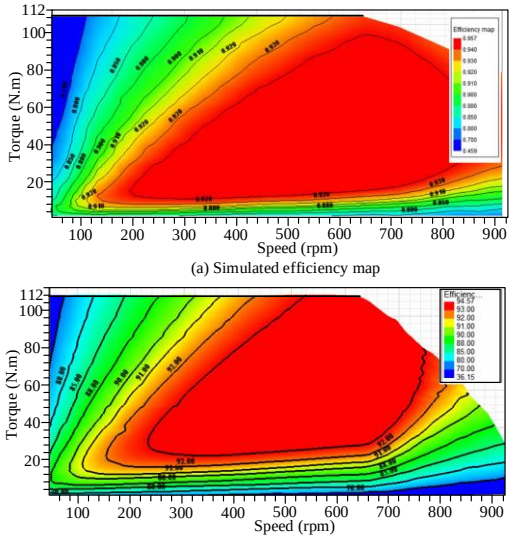

(a) Simulated efficiency map

(b) Measured efficiency map

Fig. 20. Simulated efficiency map Measured efficiency map.

In addition, the prototype motor is also installed on the test EV for load test, as shown in Fig. 19. In road test, the prototype can satisfy the dynamic requirements of vehicles under many driving conditions. Finally, Fig. 20 shows the simulated and measured efficiency maps for proposed PMSHM. As shown, the efficiency of the motor in the main working area is above 90%. During the starting condition the efficiency of the motor is above 80%. And the measured results are basically consistent with the simulation results.

VII. Conclusion

Taking suspension stability and rotating speed regulation into consideration simultaneously is an important topic in BPMSM system. In this paper, a state feedback controller tuned by GWO is proposed with good tracking and disturbance suppression performance. Compared with traditional SFC, the proposed strategy does well with less response time and stable traceability by using GWO optimization, which also shows the obvious advantages in regard to the computational efficiency and avoiding local optimization. Moreover, the overshoot is successfully rejected, resulting from the introduction of the penalty coefficient to the fitness index. The proposed strategy is verified by the simulations and experimental BPMSM system where three other controllers, TSFC, 1SFC and GP, are also given for comparison. And the results show that the proposed strategy has the best superiority in the stability of rotor position and rotating speed after one of them mutated. Besides, the disturbance inhibition is also guaranteed.

In this paper, the multi-objective optimization design, duty-cycle model predicate current control and performance verification of an outer rotor PMSHM for a low-speed direct drive EV were carried out. Firstly, in order to ensure that the designed motor meets the requirements of vehicle driving conditions, the driving cycle was sampled. The high frequency working points during the driving cycle are classified, and the basic technical requirements of motor design are obtained. Secondly, the preliminary design of the motor was carried out, and two alternative schemes were given. Thirdly, Kriging model and NSGA II algorithm were used to optimize the design of the two alternative models. In addition, the FEM and temperature network model were used to verify the optimization results to determine the feasibility of the optimization model. The optimization results were compared to select the final design scheme and structural parameters. Through optimization, the comprehensive efficiency of the motor is effectively improved, the torque ripple was reduced, and the temperature rise of the motor was ensured in a reasonable range. In addition, the control strategy-DCMPCC adopted in this study can provided excellent steady state and dynamic performance under different operation condition. Finally, the prototype was tested on a bench. The test results show that the measured results of prototype agree with the simulation design results. The prototype meets the basic operating conditions of the EV, and the temperature rise is controlled within a reasonable range.

References

[1] X. Liu, H. Chen, J. Zhao, and A. Belahcen, "Research on the performances and parameters of interior PMSM used for electric vehicles," *IEEE Trans. Ind. Electron.*, vol. 63, no. 6, pp. 3533-3545, 2016.

[2] X. Sun, K. Diao, G. Lei, Y. Guo, and J. Zhu, "Real-time HIL emulation for a segmented-rotor switched reluctance motor using a new magnetic

equivalent circuit," *IEEE Trans. Power Electron.*, vol. 35, no. 4, pp. 3841-3849, Apr. 2020.
[3] X. Sun, K. Diao, G. Lei, Y. Guo, and J. Zhu, "Study on Segmented-rotor switched reluctance motors with different rotor pole numbers for BSG system of hybrid electric vehicles," *IEEE Trans. Veh. Technol*., vol. 68, no. 6, pp. 5537-5547, 2019.
[4] Z. Shi, *et al*, "Torque analysis and dynamic performance improvement of a PMSM for EVs by skew angle optimization," *IEEE Trans. Appl. Supercon*., vol. 29, no. 2, pp. 1-5, 2019.
[5] X. Sun, J. Cao, G. Lei, Y. Guo, and J. Zhu, "Speed sensorless control for permanent magnet synchronous motors based on finite position set," *IEEE Trans. Ind. Electron.*, vol. 67, no. 7, pp. 6089-6100, Jul. 2020.
[6] D. Fodorean, L. Idoumghar, M. Brévilliers, P. Minciunescu, and C. Irimia, "Hybrid differential evolution algorithm employed for the optimum design of a high-speed PMSM used for EV propulsion," *IEEE Trans. Ind. Electron*., vol. 64, no. 12, pp. 9824-9833, 2017.
[7] X. Zhu, W. Wu, L. Quan, Z. Xiang, and W. Gu, "Design and multi-objective stratified optimization of a less-rare-earth hybrid permanent magnets motor with high torque density and low cost," I*EEE Trans. Energy Convers.*, vol. 34, no. 3, pp. 1178-1189, 2019.
[8] Q. Li, T. Fan, Y. Li, Z. Wang, X. Wen, and J. Guo, "Optimization of external rotor surface permanent magnet machines based on efficiency map over a target driving cycle," in *2017 20th International Conference on Electrical Machines and Systems (ICEMS)*, 2017, pp. 1-5.
[9] L. Chen, J. Wang, P. Lazari, and C. Xiao, "Optimizations of a permanent magnet machine targeting different driving cycles for electric vehicles," *in 2013 International Electric Machines & Drives Conference*, 2013, pp. 855-862.
[10] M. Salameh, I. P. Brown, and M. Krishnamurthy, "Fundamental evaluation of data clustering approaches for driving cycle-based machine design optimization," *IEEE Trans. Transport. Electrific.*, vol. 5, no. 4, pp. 1395-1405, 2019.
[11] A. Fatemi, N. A. O. Demerdash, T. W. Nehl, and D. M. Ionel, "Large-Scale design optimization of pm machines over a target operating cycle," *IEEE Trans. Ind. Appl*., vol. 52, no. 5, pp. 3772-3782, 2016.
[12] A. Fatemi, D. M. Ionel, M. Popescu, Y. C. Chong, and N. A. O. Demerdash, "Design optimization of a high torque density spoke-type PM motor for a formula e race drive cycle," *IEEE Trans. Ind. Appl.*, vol. 54, no. 5, pp. 4343-4354, 2018.
[13] P. Kakosimos and H. Abu-Rub, "Predictive speed control with short prediction horizon for permanent magnet synchronous motor drives," *IEEE Trans. Power Electron*., vol. 33, no. 3, pp. 2740-2750, 2018.
[14] X. Zhang, L. Zhang, and Y. Zhang, "Model predictive current control for pmsm drives with parameter robustness improvement," *IEEE Trans. Power Electron.*, vol. 34, no. 2, pp. 1645-1657, 2019.
[15] X. Sun, C. Hu, Gang Lei, Y. Guo, and J. Zhu, "State feedback control for a PM hub motor based on grey wolf optimization algorithm," *IEEE Trans. Power Electron.*, vol. 35, no. 1, pp. 1136-1146, Jan. 2020.
[16] J. J. Justo, F. Mwasilu, E. Kim, J. Kim, H. H. Choi, and J. Jung, "Fuzzy model predictive direct torque control of ipmsms for electric vehicle applications," *IEEE/ASME Trans. Mechatron.*, vol. 22, no. 4, pp. 1542-1553, 2017.
[17] X. Sun, M. Wu, G. Lei, Y. Guo, and J. Zhu, "An improved model predictive current control for PMSM drives based on current track circle," *IEEE Trans. Ind. Electron.*, 2020, DOI: 10.1109/TIE.2020.2984433.
[18] M. Preindl and S. Bolognani, "Model predictive direct torque control with finite control set for pmsm drive systems, part 1: maximum torque per ampere operation," *IEEE Trans. Ind. Inform.*, vol. 9, no. 4, pp. 1912-1921, 2013.
[19] A. Fraser, "In-wheel electric motors: the packaging and integration challenges," *in Proc. CTI Symp.*, Dec. 2011.
[20] P. Ponomarev, M. Polikarpova, and J. Pyrhönen, "Thermal modeling of directly-oil-cooled permanent magnet synchronous machine," *in 2012 International Conference on Electrical Machines*, 2012, pp. 1882-1887.
[21] C. Sciascera, P. Giangrande, L. Papini, C. Gerada, and M. Galea, "Analytical thermal model for fast stator winding temperature prediction," *IEEE Trans. Ind. Electron.*, vol. 64, no. 8, pp. 6116-6126, 2017.
[22] K. Diao, X. Sun, G. Lei, Y. Guo, and J. Zhu, "Multiobjective system level optimization method for switched reluctance motor drive systems using finite element model," *IEEE Trans. Ind. Electron.*, 2020, DOI: 10.1109/TIE.2019.2962483.
[23] X. Sun, Z. Shi, G. Lei, Y. Guo, and J. Zhu, "Multi-objective design optimization of an IPMSM based on multilevel strategy," *IEEE Trans. Ind. Electron.*, 2020, DOI: 10.1109/TIE.2020.2965463.
[24] H. T. Nguyen and J. Jung, "Finite control set model predictive control to guarantee stability and robustness for surface-mounted pm synchronous motors," *IEEE Trans. Ind. Electron.*, vol. 65, no. 11, pp. 8510-8519, 2018.
[25] Y. Zhang, D. Xu, J. Liu, S. Gao, and W. Xu, "Performance improvement of model-predictive current control of permanent magnet synchronous motor drives," *IEEE Trans. Ind. Appl.*, vol. 53, no. 4, pp. 3683-3695, 2017.

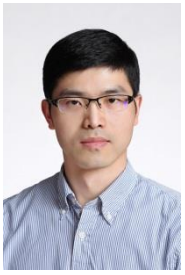

Xiaodong Sun (M'12-SM'18) received the B.Sc. degree in electrical engineering, and the M.Sc. and Ph.D. degrees in control engineering from Jiangsu University, Zhenjiang, China, in 2004, 2008, and 2011, respectively.

Since 2004, he has been with Jiangsu University, where he is currently a Professor with the Automotive Engineering Research Institute. From 2014 to 2015, he was a Visiting Professor with the School of Electrical, Mechanical, and Mechatronic Systems, University of Technology Sydney, Sydney, Australia. His current teaching and research interests include electrical machines and drives, drives and control for electric vehicles, and intelligent control. He is the author or coauthor of more than 80 refereed technical papers and one book, and he is the holder of 36 patents in his areas of interest.

Zhou Shi was born in Nantong, Jiangsu, China, in 1993. He received the B.S. degree in vehicle engineering from Jiangsu University, Zhenjiang, China, in 2016, and he is currently working toward the Ph.D. degree in Jiangsu University, Zhenjiang, China.

His current research interests include design, optimization, magnetic equivalent circuits modeling, control, and loss analysis of permanent magnet synchronous motors for automobile application.

Yingfeng Cai (M'17) received the B.S., M.S. and Ph.D. degree all from the School of Instrument Science and Engineering, Southeast University, Nanjing, China, respectively. In 2013, she joined the Automotive Engineering Research Institute in Jiangsu University, now she is a professor. Her research interests include computer vision, intelligent transportation systems and intelligent automobiles.

Gang Lei (M'14) received the B.S. degree in Mathematics from Huanggang Normal University, China, in 2003, the M.S. degree in Mathematics and Ph.D. degree in Electrical Engineering from Huazhong University of Science and Technology, China, in 2006 and 2009, respectively. He is currently a senior lecturer at the School of Electrical and Data Engineering, University of Technology Sydney (UTS), Australia. His research interests include design optimization and control of electrical drive systems and renewable energy systems.

Youguang Guo (S'02-M'05-SM'06) received the B.E. degree from Huazhong University of Science and Technology, China in 1985, the M.E. degree from Zhejiang University, China in 1988, and the Ph.D. degree from University of Technology, Sydney (UTS), Australia in 2004, all in electrical engineering. He is currently an associate professor at the School of Electrical and Data Engineering, University of Technology Sydney (UTS). His research fields include measurement and modeling of properties of magnetic materials, numerical analysis of electromagnetic field, electrical machine design optimization, power electronic drives and control.

Jianguo Zhu (S'93–M'96–SM'03) received the B.E. degree in 1982 from

Jiangsu Institute of Technology, Jiangsu, China, the M.E. degree in 1987 from Shanghai University of Technology, Shanghai, China, and the Ph.D. degree in 1995 from the University of Technology Sydney (UTS), Sydney, Australia, all in electrical engineering. He was appointed a lecturer at UTS in 1994 and promoted to full professor in 2004 and Distinguished Professor of Electrical Engineering in 2017. At UTS, he has held various leadership positions, including the Head of School for School of Electrical, Mechanical and Mechatronic Systems and Director for Centre of Electrical Machines and Power Electronics. In 2018, he joined the University of Sydney, Australia, as a full professor and Head of School for School of Electrical and Information Engineering. His research interests include computational electromagnetics, measurement and modelling of magnetic properties of materials, electrical machines and drives, power electronics, renewable energy systems and smart micro grids.